STScI | SPACE TELESCOPE SCIENCE INSTITUTE

Instrument Science Report ACS 2018-09

ACS/WFC Parallel CTE from EPER Tests

J. E. Ryon, N. A. Grogin

December 20, 2018

Abstract

We present a new analysis of parallel charge transfer efficiency (CTE) in ACS/WFC over its operational lifetime. We utilize extended pixel edge response (EPER) data to monitor the signal and time dependence of CTE in the WFC CCDs, taking a similar approach to Mutchler & Sirianni (2005). We find that CTE has a power law dependence on signal level, such that CTE is worst for low signal levels and best for high signal levels. We also find that CTE decreases linearly with time. The rate of decrease is higher for low signal levels, but may be flattening in recent data at higher signal levels. Monitoring and comparison to other CTE studies will continue for the rest of ACS's lifetime.

1 Introduction

The charge transfer efficiency (CTE) of the ACS/WFC CCDs has been decreasing over the operational lifetime of the instrument, due to the radiation damage in space. Charge traps in the silicon lattice are localized in CCD pixels and trap electrons as charge is transferred during readout. Traps release this charge on timescales comparable to the parallel transfer rate of readout, displacing electrons from the source into exponentially-decreasing charge trails.

Two methods for correcting for imperfect CTE have been developed by the ACS Team, the empirical photometric correction of Chiaberge (2012) and the pixel-based image reconstruction technique of Anderson & Bedin (2010) and Anderson & Ryon (2018). Regular

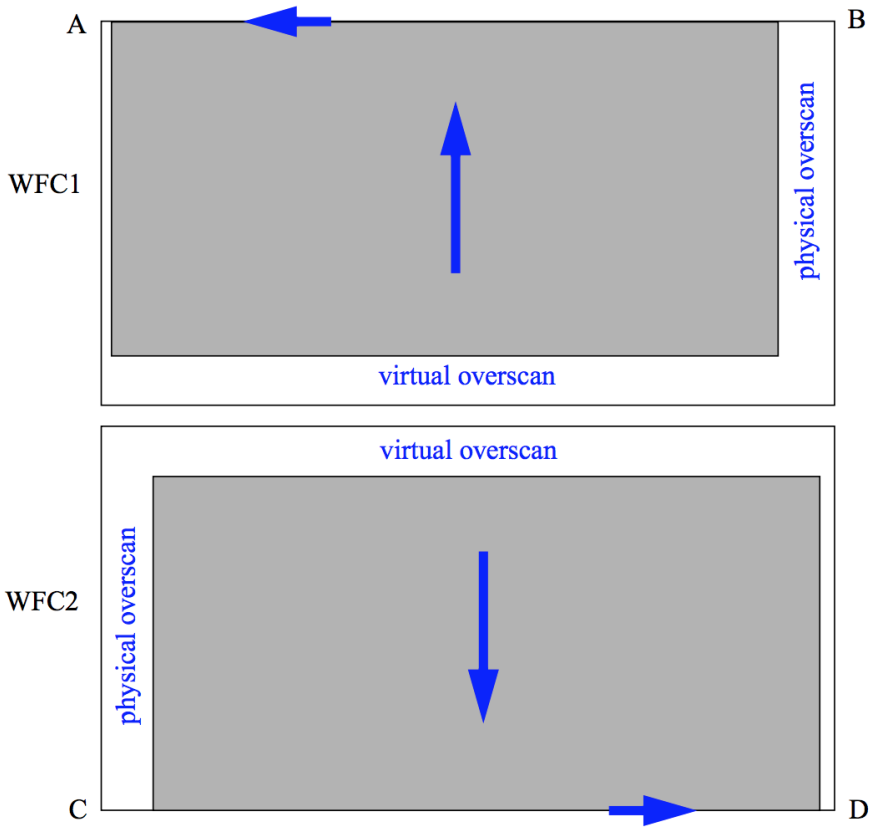

Figure 1: Format of a WFC EPER frame read out using amplifiers A and D, reproduced from Mutchler & Sirianni (2005). The vertical and horizontal arrows indicate the parallel and serial transfer directions, respectively, for each chip. The gray shaded region represents the exposed pixels. The physical prescans nearest the readout amplifiers (A and D) contain 24 columns, whereas the physical overscans furthest from the amplifiers contain 75 columns. The virtual overscans contain 75 rows.

monitoring of the decay of CTE is performed by the Internal and External CTE Monitoring programs. The External program obtains observations of 47 Tuc to monitor the decay of CTE and update the photometric correction of Chiaberge (2012). The Internal program obtains extended pixel edge response (EPER) images to monitor how CTE depends on time and signal level. Because the EPER test is not influenced by effects like sky background and focus variations, it provides an independent check of the External monitor.

Mutchler & Sirianni (2005) provide a detailed description of the EPER test and results from March 2002 through October 2004. We briefly describe the data and reasoning behind EPER tests here. EPER frames are essentially flat fields, in that the WFC CCDs are illuminated by the Tungsten calibration lamp. Combinations of filters and exposure times are used to reach a range of signal levels. A special readout mode (header keyword `CTEIMAGE` = `EPER`) uses a single amplifier to read out each chip and clock the overscans for many additional transfers. As shown in Figure 1, the resulting frame for a single chip is 4195×2123 pixels in size, with 24 columns of physical prescan on the leading edge (nearest to the amplifier), 75 columns of physical overscan on the trailing edge (furthest from the

amplifier), and 75 rows of virtual overscan[1]. As readout proceeds, imperfect CTE, in both the parallel and serial transfer directions, displaces charge from the exposed pixels into the extra-large overscans. This "deferred" charge appears as an exponentially-decreasing trail as charge traps release their trapped electrons. According to Janesick (2001), comparing the deferred charge, ΔQ, to the signal level of the exposed pixels, Q, provides an estimate of the average CTE per pixel for that signal level,

$$\mathrm{CTE} = 1 - \frac{\Delta Q}{2048 Q}. \tag{1}$$

The EPER test is considered a relative CTE technique because it does not directly measure charge lost from a source, which would require a priori knowledge of the source flux. The Fe^{55} test, which uses a radioactive source to generate 5.89 keV X-rays that appear as 1620 e^- charge packets in CCDs, is an example of an absolute CTE test (Janesick, 2001). This test was performed during ground testing of the WFC CCDs to establish the initial, absolute CTE values, which are presented in Table 4.7 in the ACS Instrument Handbook (Ryon & et al., 2018). However, because the EPER test is entirely internal to the instrument and requires few orbits, it is relatively cheap in terms of observatory operations. In addition, if the deferred charge and exposed pixel signal level are measured in a consistent manner in all EPER data, then the CTE measurements can be compared to each other. The EPER test has therefore formed the basis of the Internal CTE Monitor calibration program in use since ACS's installation, as discussed in Section 2.

This study presents a new analysis of parallel CTE in all ACS/WFC EPER frames. We will investigate serial CTE in future study. We describe the data used in Section 2. In Section 3, we describe our method for measuring CTE by fitting the shape of the deferred charge trail. We explore how CTE depends on time and signal level in Section 4. The results from this study are summarized in Section 5.

2 Data

EPER data for WFC have been obtained at least once per year since the installation of ACS, excluding the period from January 2007 to May 2009 when WFC was not operational. Details of the programs that obtained WFC EPER observations can be found in Table A1 in the Appendix. The first EPER data come from the Servicing Mission Orbital Verification (SMOV) period shortly after ACS was installed during Servicing Mission 3B (SM3B) in March 2002. The Internal CTE Monitor program[2] initially obtained monthly EPER observations over a range of signal levels. In 2004, monthly monitoring of the same signal level

[1]The ACS CCDs have 24 physical pixels located between the serial register and each amplifier. The physical prescan region is produced by reading out these 24 pixels before each row of exposed pixels. The trailing physical overscan region is produced by performing 75 serial transfers, using the 24 physical pixels at the end of the serial register, after each row of exposed pixels. The trailing virtual overscan region is produced by performing an additional 75 parallel transfers of the exposed pixel array.

[2]This program also obtained EPER data for HRC and First Pixel Response (FPR) data for both cameras. The FPR test is another method for estimating CTE, but it only measures serial CTE for WFC. FPR data was removed from the program post-SM4 to reduce the number of orbits required for the program, so we do not include it in this study.

as the Fe^{55} test (1600 e^-) was moved to the CCD Hot Pixel Annealing program, and the Internal CTE Monitor obtained once-yearly EPER data of a range of signal levels. After two small EPER programs were executed during SMOV for Servicing Mission 4 (SM4) in spring 2009, the pre-SM4 monitoring resumed until 2010. EPER data of a range of signal levels were then obtained once yearly until 2015, when the frequency was increased to twice per year. Each epoch of EPER data (excluding SM3B SMOV) includes 1620 e^- for comparison to the Fe^{55} test.

Prior to 2009, EPER data were taken using amp AD and BC readout. Only amp AD was used afterwards, which is illustrated in Figure 1. BC readout is the mirror image of Figure 1, in that WFC1 is read out with amp B and WFC2 is read out with amp C. According to Mutchler & Sirianni (2005), the reason for taking data with both amplifier pairs is to test whether readout direction has any effect on the charge traps, and they find none[3]. In the same vein, WFC1 and WFC2 should have very similar CTE characteristics because they were cut from the same material and have experienced similar bombardment by space radiation.

EPER data cover a wide range of signal levels, from 180 e^- to 52,000 e^-, as shown in Table A2. The lower levels are obtained by crossing the F555W and F435W filters and exposing the CCDs to the Tungsten lamp for a very short time. The higher levels use only the F435W filter. During our analysis, we found a small amount of excess signal in the last overscan rows that could not be explained by bias structure or dark current. We determined that it is likely due to light from the Tungsten lamp leaking through the shutter during readout, as discussed in Section 3.2.

Short (0.5079 sec) dark frames using the EPER readout mode were obtained during most pre-SM4 programs and were used as "pseudo-biases" to remove bias structure from the EPER flats, according to Mutchler & Sirianni (2005). These short darks were removed from post-SM4 programs because they were no longer used, according to the Phase II proposal of program 12386. We obtained short darks for the two most recent programs in order to estimate the effects of bias structure and readout dark (Ryon et al., 2017) on the overscans.

3 Estimating CTE from EPER Data

To calculate a value for parallel CTE from each EPER frame using Equation 1, the signal level of the exposed pixels, Q, and the deferred charge in the overscan region, ΔQ, must be measured.

3.1 Data Reduction

We first perform a basic data reduction because the EPER readout format is not supported by CALACS. Each frame is oriented to match WFC2 read out with amp D (see Figure 1). The bias level of each frame is estimated by sigma-clipping and averaging a 65×10 pixel rectangle in the overlap region of the virtual overscan and physical prescan. This rectangle lies in the top left corner of the overlap region, and as such, it is the EPER-readout equivalent of the area identified in Figure 8 of Golimowski et al. (2011) as least affected by bias shift.

[3]We note that the only change in direction between AD and BC readout takes place at the serial register, and therefore should only test whether serial CTE has any dependence on direction.

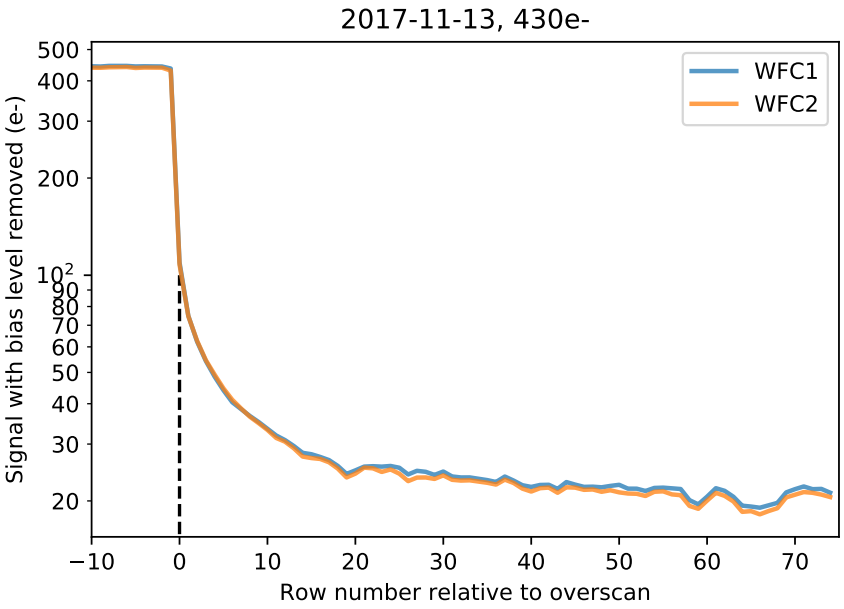

Figure 2: Average column for WFC1 (blue curve) and WFC2 (orange curve) for a 430 e^- EPER frame from the November 13, 2017 anneal cycle. The last 10 rows of exposed pixels and all 75 virtual overscan pixels are shown. The dashed black line marks the first row of overscan pixels, which is where the deferred charge trails begin. Only the bias level has been removed from this profile.

The rectangle also contains enough rows such that the bias striping noise is mitigated when averaged. The bias level is subtracted from the frame while both are in units of DN, and then the frame is multiplied by the gain appropriate for the amplifier to convert to electrons. We perform no further bias or dark calibration to the EPER data at this stage.

Next, hot columns more than 3×NMAD[4] from the median level in the overscan rows furthest from the exposed pixels are removed from the frame. Cosmic rays are removed by sigma-clipping along each row and growing each deviant pixel by two pixels in all directions. For Figure 2, the remaining pixels are average-combined along the rows to produce an average column for each chip from a November 2017 430 e^- EPER frame. The last 10 exposed pixels have a nearly constant signal level, and the 75 pixels of virtual overscan show an exponentially-decreasing charge trail with some variation caused by bias-striping noise.

3.2 Light Leaks and Amp Dependence

In Figure 2, the deferred charge trail in the overscan pixels does not decay to zero electrons towards the edge of the chip (row 75), rather, there is a pedestal of ∼20 e^- remaining. We expect a pedestal to remain because there is 2D structure in the bias and dark current accumulated during readout that cannot be accounted for by the bias level subtraction alone. The bias structure is particularly strong post-SM4 Golimowski et al. (2011). Dark current accumulated during readout, called readout dark, is about twice as large as a typical ACS/WFC frame because the read time of an EPER frame is about twice as long (Ryon

[4]Normalized median absolute deviation, a robust estimate of the standard deviation when there are strong outliers.

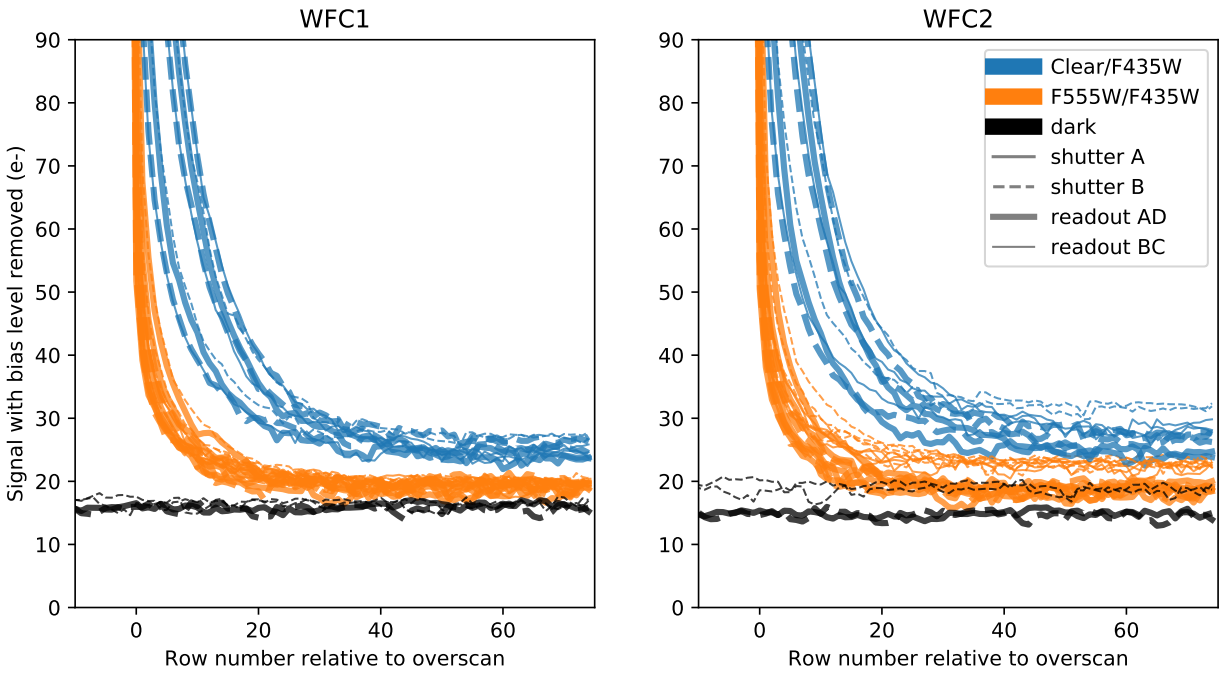

Figure 3: Average overscan columns for data from program 11881, observed in October 2009, for WFC1 (left) and WFC2 (right). Orange curves represent data taken with the F555W/F435W filter pair, and blue curves represent data taken with the F435W filter alone. Black curves represent short dark images. Solid (dashed) lines represent shutter position A (B). Thick (thin) lines represent amp AD (BC) readout.

et al., 2017). Readout dark rate has been increasing over the lifetime of ACS/WFC, so the pedestal in the EPER overscans has also been increasing with time (e.g., from $\sim$5 e^- to 20 e^- for the signal level of the data in Figure 2). If these sources of extra signal are accounted for, we expect the overscan column to decay to zero because charge traps in each column should release their trapped electrons into the overscan pixels on short timescales.

Short dark frames should contain the same bias structure and readout dark as the EPER frames from the same program because they use the same readout mode. They can therefore be used to determine if other sources are contributing signal to the overscan pedestals. The short dark frames are processed in the same manner as the EPER frames, and the overscan rows are then average-combined into a single column.

In Figure 3, we plot the average overscan columns of the EPER data and short darks from October 2009 (PID 11881). The lower signal level frames, which use the F555W/F435W filter pair, are represented by orange curves, and the higher signal levels by blue curves, which use F435W alone. The black curves show the overscans of the short darks. While most of the pedestal in the EPER overscans is also present in the short dark overscans, there remains a clear offset towards the edge of the chip (row 75). This means that the signal in the EPER overscans is not entirely accounted for by bias structure or readout dark. In addition, the EPER curves appear to cluster by filter pair towards the edge of the chip for both WFC1 and WFC2. Lower-level splitting of the orange and blue groups into solid and dashed lines, which represent the A and B shutter position, respectively, is also visible. There is little difference in the pedestals between the curves of the same filter and shutter combination

Table 1: Results of CTE analysis for EPER frame `jdima2cmq` from November 2017 (PID 14950)

Chip/Amp	Q **(e$^-$)**	ΔQ **(e$^-$)**	**CTE**	**CTE 84th percentile**	**CTE 16th percentile**	$q_{\rm ped}$ **(e$^-$)**	$\mathbf{t_1}$ **(pix)**	$\mathbf{t_2}$ **(pix)**
WFC1/A	427.2	450.0	0.99948	3.8×10^{-5}	3.7×10^{-5}	22.1	9.2	1.3
WFC2/D	422.7	455.0	0.99947	3.5×10^{-5}	5.4×10^{-5}	21.4	8.7	1.2

despite differences of hundreds or even several thousand electrons of signal level, suggesting that these effects are not simply due to CTE differences between signal levels.

This behavior suggests that light is leaking through the closed shutter during readout. In fact, the Tungsten lamp turns on before each EPER exposure and does not turn off until a few minutes after readout is completed (private communication, Thomas Wheeler). Based on analysis of the offset between the short dark and EPER overscans, the amount of light leaking onto the chip depends on the filter pair and shutter in the optical path. This points to the lamp being the source of the extra signal. The amount of light leakage for each filter and shutter combination is fairly constant over time. If the offset between the dark and EPER overscans was increasing with time, then there could be another source of signal, such as charge traps that release electrons on long timescales. Our analysis suggests that there are few, if any, of these charge traps in ACS/WFC.

Finally, in the WFC2 panel, even further splitting occurs according to thick versus thin lines, which represent AD and BC readout, respectively. A similar splitting is seen in the darks. This could imply that post-SM4, the bias structure in amp C is much more substantial than amp D, or that serial CTE is dependent on readout direction for WFC2. An in-depth investigation of the latter will be conducted in the future.

3.3 Calculating CTE

We can now find the average CTE per pixel for each EPER frame. The signal level in the exposed pixels in each EPER frame varies quite substantially in the serial (x) direction. The overscan pixels vary less strongly, but both variations affect the accuracy of the CTE values from each frame. To include this variation but increase the signal-to-noise for our fits, we create 16-column-wide bins across the frame and take the average along each row of the bin to find the average column.

We then find the distribution of Q values from the exposed pixels in the frame. To do this, we fit a line to each binned column, i, in the 75 rows of exposed pixels nearest to the overscan. The fitted value at the edge of the exposed region (row 2048) is the signal level for that column, Q_i.

Next, we find the distribution of ΔQ values from the overscans. In each binned column of the 75 rows of overscan pixels, the deferred charge trail is fit with a function of the form

$$q(x) = q_{\rm ped} + a\,{\rm e}^{-x/t_1} + b\,{\rm e}^{-x/t_2}, \tag{2}$$

where the free parameters are $q_{\rm ped}$, a, t_1, b, and t_2. We use `scipy.optimize.curve_fit` to perform the fitting for both Q_i and $q_i(x)$, and we require the free parameters for $q_i(x)$ to be positive. An example of this fit is shown in Figure 4. The parameter $q_{\rm ped}$ is the pedestal

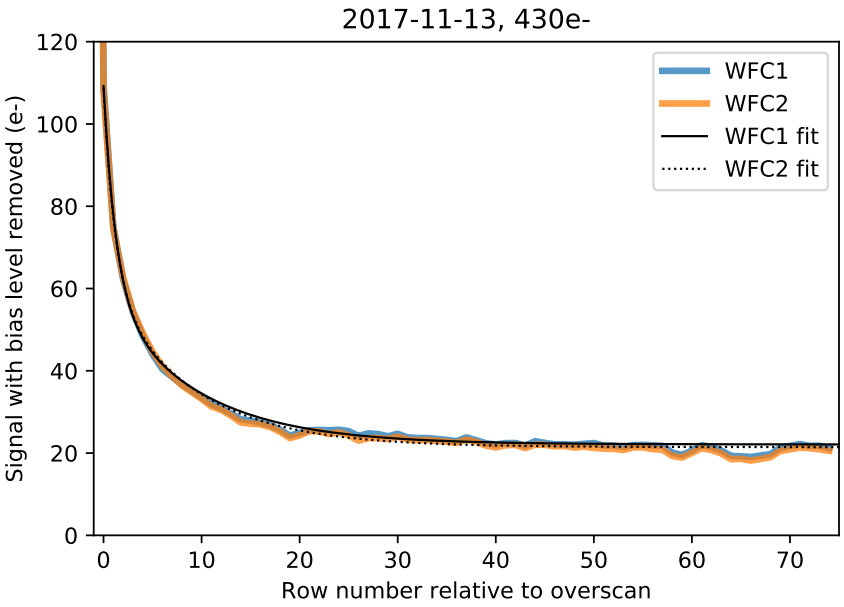

Figure 4: Same as in Figure 2 with double exponential fits to both WFC1 and WFC2 overscans plotted as solid and dashed lines, respectively. Equation 2 is the functional form of the fits.

remaining after bias level subtraction and t_1 and t_2 represent trap release timescales in units of pixel transfers.

In Section 3.2, we determined that the pedestal $q_{\rm ped}$ consists of bias structure, readout dark, and light leak from the lamp, and therefore should be removed. The pedestal $q_{\rm ped}$ is subtracted from Q_i and from each pixel of the fitted charge trail $q_i(x)$. Then, $q_i(x)$ is summed over the 75 overscan pixels to find ΔQ_i. Finally, CTE$_i$ is calculated for each binned column according to Equation 1. We find the median and the 16th and 84th percentiles ($\sim 1\sigma$) of the distribution of CTE values for each chip in each EPER frame. Because many EPER programs have obtained multiple exposures of a given signal level, there are often several CTE measurements per signal level.

In Table 1, we present the results of these fits for the EPER frame from November 2017 used in Figures 2 and 4. The measurements agree well between the two chips. Note that there are more electrons in the deferred charge trail than the signal level of the frame. As shown in Anderson & Ryon (2018), there are more traps available to charge packets of size $\lesssim$300 e$^-$ than electrons in the charge packets themselves. A single charge packet, such as a hot pixel, would not be able to fill all of the charge traps in a column below 300 e$^-$. However, a series of charge packets of similar size, like a column of exposed pixels in an EPER frame, could fill all available charge traps within a few transfers and would refill the traps as electrons are released during readout. Then, all of the trapped electrons are released into the EPER overscan, leading to more charge in the deferred charge trails of low signal level EPER frames than signal.

Because Equation 2 fits the EPER overscans well, the charge traps in ACS/WFC appear to exist in two populations, one that releases charge after about 1 pixel transfer, and another that releases charge after about 10 transfers. These trap release timescales agree well with those reported in Massey (2010) from their analysis of warm pixels.

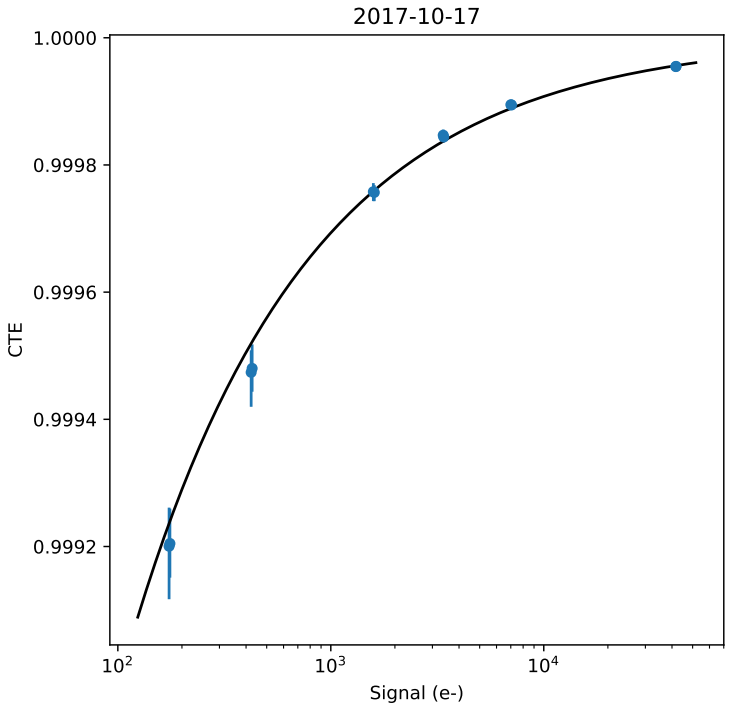

Figure 5: Parallel CTE as a function of signal level in electrons for EPER data from the 2017-10-17 anneal cycle. The black line represents a power law fit (Equation 3) to the data.

Table 2: Pre- and post-SM4 power law fit results

Epoch	n	c	p
Pre-SM4	$6.8\times10^{-5} \pm 4\times10^{-6}$	$1.66\times10^{-6} \pm 4\times10^{-8}$	-0.528 ± 0.003
Post-SM4	$-1.3\times10^{-4} \pm 6\times10^{-5}$	$2.00\times10^{-6} \pm 3\times10^{-8}$	-0.521 ± 0.002

4 Evolution of CTE Measurements

Figure 5 shows parallel CTE as a function of signal level for EPER data obtained during the 2017-10-17 anneal cycle. The CTE values measured from both WFC1 and WFC2 are plotted along with their 84th and 16th percentiles as error bars, and show good agreement at each signal level. CTE dependence on signal level takes a power law shape, with the worst (best) CTE corresponding to the lowest (highest) signal levels. Following Mutchler & Sirianni (2005), a power law model describing the evolution of CTE is

$$\mathrm{CTE}(s,d) = 1.0 - (n + c(d - 52335))s^p, \tag{3}$$

where s is the signal level, d is the MJD of the observation, p is the power law exponent, and n and c are the intercept and slope of the time dependence, respectively. The MJD 52335 corresponds to the launch date of SM3B, the beginning of ACS's operational lifetime.

We group the CTE measurements from each program by anneal date, and each group with more than two signal levels is fit with Equation 3 using `scipy.optimize.curve_fit`. The 84th and 16th percentiles of the CTE measurements are included as errors on the fit.

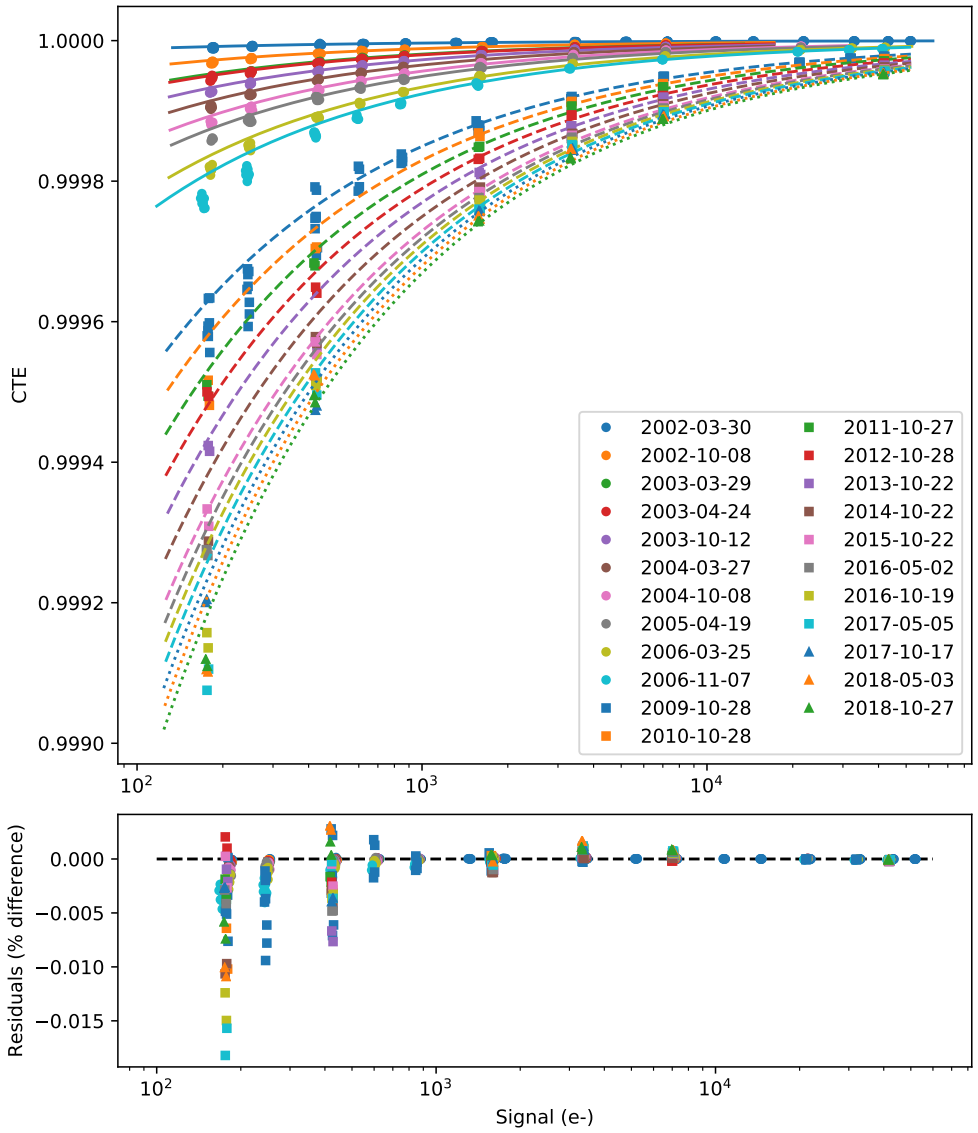

Figure 6: Parallel CTE as a function of signal level (top) and residuals as a function of signal level (bottom) for programs that obtained data at more than two signal levels. Each set of data is labeled by the anneal date of the observations. The circles represent pre-SM4 data, and the squares and triangles post-SM4 data. Both WFC1 and WFC2 results are plotted with the same symbols. The color-matched curves are the best-fit power law models evaluated at the anneal date of the datasets. The solid curves represent pre-SM4 model fits and the dashed and dotted curves both represent post-SM4 model fits.

In Figure 5, the CTE errors are larger for lower signal level data, so the fitting routine gives less weight to those points and leads to the two lowest signal level points falling below the curve. Across all EPER programs, the best-fit power law exponent, p, ranges in value from -0.43 to -0.59. Because n and c control the time dependence of the power law model, they are very uncertain for each individual anneal.

To better constrain the model's time dependence, we group the CTE measurements into pre-SM4 and post-SM4 observations. Using all of the data in each group, we perform a multivariate fit over both signal level and date (Equation 3) The results of these fits are

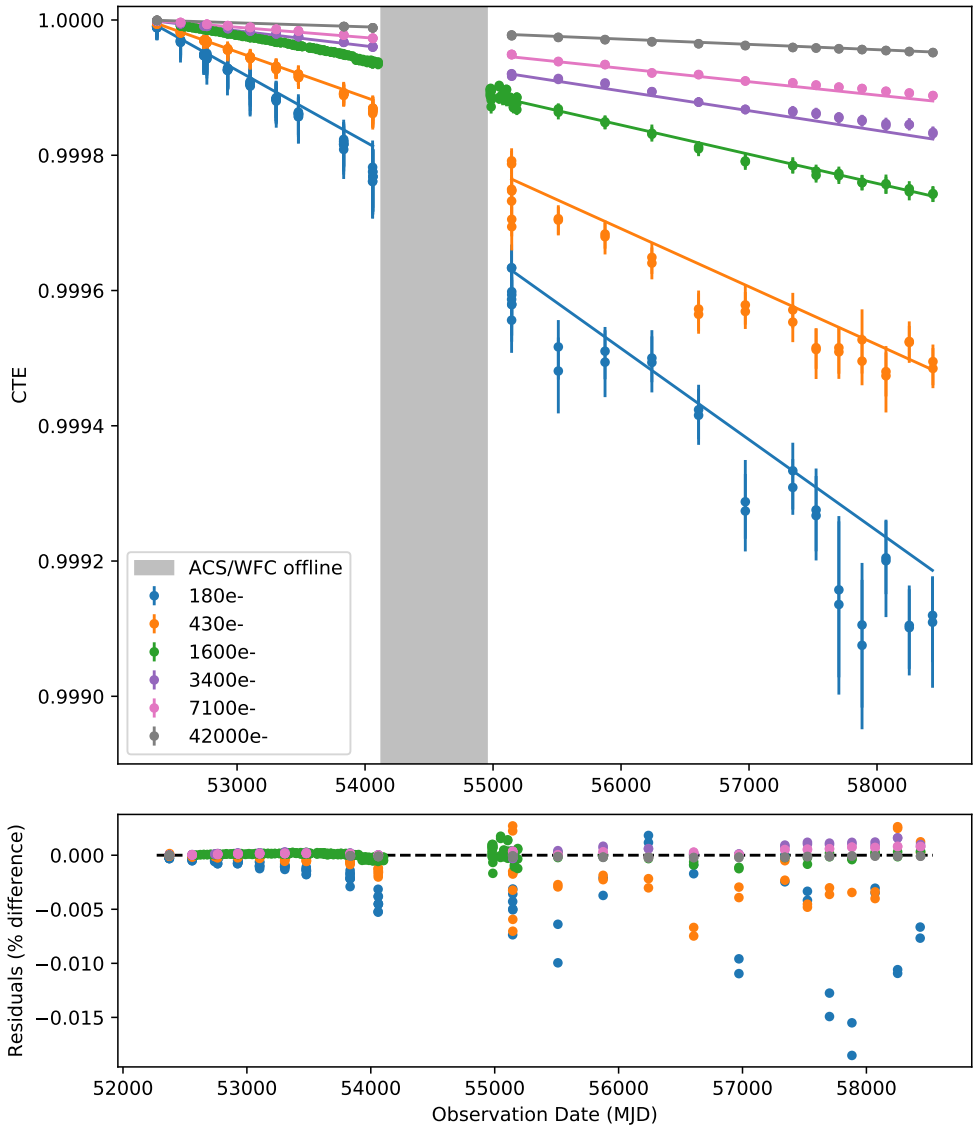

Figure 7: Parallel CTE as a function of time (top) and residuals as a function of time (bottom) for programs that obtained data at the labeled signal levels. Both WFC1 and WFC2 results are plotted with the same symbols. The color-matched curves are the best-fit power law models evaluated at the average signal level of the datasets, separated according to pre- and post-SM4 observation dates. The gray shaded band is the time period during which ACS/WFC was offline.

presented in Table 2. In Figure 6, we plot CTE as a function of signal level for all of the programs that obtained data at more than two signal levels. The data are labeled by the anneal in which they were obtained. The curves are the best-fit pre- and post-SM4 power law models fixed to the anneal date of each set of data. We plot the residuals, as percent difference, between the data and the model in the bottom panel.

In Figure 7, we plot CTE as a function of observation date for signal levels that have been obtained regularly since SM4. The lines are the same best-fit power law models from Figure 6 for both pre- and post-SM4, but here are evaluated at the average signal levels labeled in

Table 3: CTE time dependence

Signal Level (e^-)	Change in CTE per year	Change in CTE per year from Anderson & Ryon (2018)
180	-4.9×10^{-5}	-4.6×10^{-5}
430	-3.1×10^{-5}	-2.7×10^{-5}
1600	-1.5×10^{-5}	-1.3×10^{-5}
3400	-1.1×10^{-5}	-9.1×10^{-5}
7100	-7.2×10^{-6}	-6.4×10^{-6}
42000	-2.9×10^{-6}	-2.9×10^{-6}

the figure. We again present the residuals in the bottom panel. In both Figures 6 and 7, the WFC1 and WFC2 results are plotted together and show good agreement. The lower signal level data fall below the model trend, especially in recent observations. In these data, the typical pixel encounters more traps than it has signal, which leads to high uncertainty in the CTE value and may mean that the power law signal dependence in Equation 3 no longer describes the low signal level data well. However, the linear time dependence still generally describes the data well, though the trend appears to be becoming shallower for the >1600 e^- signal levels recently.

The post-SM4 rate of decrease of CTE for each of the signal levels plotted in Figure 7 is given in Table 3. We also provide the same measure determined from the trap density profile and time dependence of the pixel-based CTE model from Anderson & Ryon (2018). The rates of decrease agree well between the two independent methods of determining CTE.

5 Conclusions

In this study, we present a new analysis of ACS/WFC parallel CTE from EPER data. Our analysis agrees with many of the results of Mutchler & Sirianni (2005), in that CTE losses are highest at low signal levels, and CTE has a power law dependence on signal and a linear dependence on time. We also confirm the suspicion that light leaks from the Tungsten lamp contaminate the EPER overscans, and must be accounted for in the analysis. CTE values from the lowest signal level data fall below the CTE model, which may suggest that when more traps exist than signal, the model no longer describes the data well. In addition, there appears to be a flattening of the linear decrease in CTE for higher signal levels, which we will continue to monitor. Future work will use EPER data to study serial CTE in ACS/WFC.

We note that EPER data tend to overestimate the actual parallel CTE per pixel for two reasons: (1) Equation 1 is a binomial approximation to another equation, in which the CTE for each pixel transfer is multiplied, or CTE^N, and (2) eventually the deferred charge trail will not reach the bias level within 75 pixel transfers, causing pedestal subtraction to remove real deferred charge, artificially inflating CTE. There is no clear solution to (1), but we note that measuring CTE consistently should ensure the results from different time periods are comparable. We may address (2) in the future by updating the EPER readout mode to read out substantially more virtual overscan rows. In addition, Fe^{55} tests performed before launch of SM4 showed slightly lower parallel CTE values than we find in EPER data obtained

shortly after ACS was installed. This suggests that there may be a systematic offset between the EPER CTE results and the true parallel CTE.

The procedure for measuring CTE from EPER data is now implemented in python and requires little user input. Using this implementation, the ACS team will continue to monitor CTE for the full lifetime of ACS/WFC. New signal levels may be added to the Internal CTE Monitor calibration program as it becomes more difficult to measure CTE for the lowest signal levels. While converting the EPER CTE results into a correction for observations is not practical, they provide an independent check on the signal and time dependence of external CTE tests (Chiaberge, 2012) and the pixel-based CTE correction technique (Anderson & Ryon, 2018), which ACS users are encouraged to use to correct their data.

Acknowledgements

We thank Jay Anderson and Marco Chiaberge for helpful discussions pertaining to comparison of the EPER results to their work. We also thank the following ACS team members for their helpful comments on this report: Nimish Hathi, Vera Platais, Marco Chiaberge, Ralph Bohlin, Jay Anderson, Nate Miles, and Melanie Olaes.

References

Anderson, J., & Bedin, L. R. 2010, PASP, 122, 1035

Anderson, J., & Ryon, J. E. 2018, Improving the Pixel-Based CTE-correction Model for ACS/WFC, ACS ISR 2012-04, STScI

Chiaberge, M. 2012, A new accurate CTE photometric correction formula for ACS/WFC, ACS ISR 2012-05, STScI

Golimowski, D., Cheng, E., Loose, M., et al. 2011, ACS after Servicing Mission 4: The WFC Optimization Campaign, ACS ISR 2011-04, STScI

Janesick, J. R. 2001, Scientific charge-coupled devices

Massey, R. 2010, MNRAS, 409, L109

Mutchler, M., & Sirianni, M. 2005, Internal monitoring of ACS charge transfer efficiency, ACS ISR 2005-03, STScI

Ryon, J. E., & et al. 2018, ACS Instrument Handbook, Version 17.0 (Baltimore: STScI)

Ryon, J. E., Grogin, N. A., & Coe, D. 2017, Accounting for Readout Dark in ACS/WFC Superbiases, ACS ISR 2017-13, STScI

Appendix

Table A1: Details of EPER observations from ACS/WFC calibration programs

Program ID	Anneal Date(s)	Signal Levels (e^-)	Readout Mode(s)	Dark(s) Taken?
08948[a]	2002-03-30	180, 250, 430, 610, 860, 1300, 1750, 3400, 5200, 7100, 11,000, 14,500 21,000, 32,000 42,000, 52,000	AD, BC	Y
09649	2002-08-14, 2002-09-10, 2002-10-08, 2002-11-08, 2002-12-05, 2002-12-31, 2003-01-25, 2003-03-02, 2003-03-29, 2003-04-24, 2003-05-19, 2003-06-22, 2003-08-14, 2003-09-09	180, 250, 430, 610, 860, 1200, 1600, 3400, 7100	AD, BC	Y
10044	2003-10-12, 2003-11-06, 2003-12-01, 2004-01-04, 2004-01-30, 2004-03-04, 2004-03-27, 2004-05-22, 2004-06-18, 2004-07-14, 2004-09-08	180, 250, 430, 610, 860, 1600, 3400, 7100	AD, BC	Y
10369	2004-10-08, 2005-03-24, 2005-04-19	180, 250, 430, 610, 860, 1600, 3400, 7100, 21,000	AD, BC	Y
10370	2004-09-08, 2004-10-08, 2004-11-05, 2004-12-02, 2004-12-30, 2005-01-29, 2005-03-04, 2005-03-24, 2005-04-19, 2005-05-20, 2005-07-16, 2005-08-11, 2005-09-09	1600	AD	N
10732	2006-03-25	180, 250, 430, 610, 860, 1600 3400, 7100, 21,000 32,000, 42,000	AD, BC	Y
10733	2005-09-09, 2005-10-08, 2005-11-03, 2005-11-25, 2005-12-31, 2006-01-25, 2006-03-04, 2006-03-25,	1600	AD	N

continued

Table A1: Details of EPER observations from ACS/WFC calibration programs

Program ID	Anneal Date(s)	Signal Levels (e^-)	Readout Mode(s)	Dark(s) Taken?
	2006-04-21, 2006-05-17, 2006-06-15, 2006-07-15, 2006-08-10, 2006-09-08, 2006-10-10, 2006-11-07, 2006-12-05			
11045	2006-11-07	180, 250, 430, 610, 860, 1600, 3400, 7100, 21,000, 32,000, 42,000	AD, BC	Y
11046[b]	2006-12-05, 2007-01-02	1600	AD	N
11809[c]	2009-05-27	1600, 8500	AD, BC	N
11810[c]	2009-05-27	1600, 8500	AD, BC	N
11881	2009-10-28	180, 250, 430, 610, 860, 1600 3400, 7100, 21,000 32,000, 42,000	AD, BC	Y
11882	2009-07-06, 2009-08-05, 2009-08-31, 2009-10-02, 2009-10-28, 2009-11-25, 2009-12-21	1600	AD	N
12386	2010-10-28	180, 430, 1600 3400, 7100, 42,000	AD	N
12731	2011-10-27	180, 430, 1600 3400, 7100, 42,000	AD	N
13156	2012-10-28	180, 430, 1600 3400, 7100, 42,000	AD	N
13593	2013-10-22	180, 430, 1600 3400, 7100, 42,000	AD	N
13956	2014-10-22	180, 430, 1600 3400, 7100, 42,000	AD	N
14399	2015-10-22, 2016-05-02	180, 430, 1600 3400, 7100, 42,000	AD	N
14508	2016-10-19, 2017-05-05	180, 430, 1600	AD	N

continued

Table A1: Details of EPER observations from ACS/WFC calibration programs

Program ID	**Anneal Date(s)**	**Signal Levels (e^-)**	**Readout Mode(s)**	**Dark(s) Taken?**
		3400, 7100, 42,000		
14950	2017-10-17, 2018-05-03	180, 430, 1600 3400, 7100, 42,000	AD	Y
15523[d]	2018-10-27, 2019-05-20 (scheduled)	180, 430, 1600 3400, 7100, 42,000	AD	Y

[a] Post-SM3B SMOV program
[b] Program ended prematurely due to Side 2 electronics failure
[c] Post-SM4 SMOV program
[d] Ongoing program

Table A2: Details of EPER observations of various signal levels

Signal Level (e^-)	Exposure Time (s)	Filter 1	Filter 2	Program IDs
180	0.5079	F555W	F435W	08948, 09649, 10044, 10369, 10732, 11045, 11881, 12386, 12731, 13156, 13593, 13956, 14399, 14508, 14950, 15523
250	0.6934	F555W	F435W	08948, 09649, 10044, 10369, 10732, 11045, 11881
430	1.2	F555W	F435W	08948, 09649, 10044, 10369, 10732, 11045, 11881, 12386, 12731, 13156, 13593, 13956, 14399, 14508, 14950, 15523
610	1.7	F555W	F435W	08948, 09649, 10044, 10369, 10732, 11045, 11881
860	2.4	F555W	F435W	08948, 09649, 10044, 10369, 10732, 11045, 11881
1200	3.3	F555W	F435W	09649
1300	3.6	F555W	F435W	08948
1600	4.5	F555W	F435W	09649, 10044, 10369, 10370, 10732, 10733, 11045, 11046, 11881, 11882, 12386, 12731, 13156, 13593, 13956, 14399, 14508, 14950, 15523
1750	0.5079	CLEAR1L	F435W	08948
3400	1.0	CLEAR1L	F435W	08948, 09649, 10044, 10369, 10732, 11045, 11881, 12386, 12731, 13156, 13593, 13956, 14399, 14508, 14950, 15523
5200	1.5	CLEAR1L	F435W	08948
7100	2.1	CLEAR1L	F435W	08948, 09649, 10044, 10369, 10732, 11045, 11881, 12386, 12731, 13156, 13593, 13956, 14399, 14508, 14950, 15523
8500	24.5	F555W	F435W	11809, 11810
11,000	3.1	CLEAR1L	F435W	08948
14,500	4.2	CLEAR1L	F435W	08948
21,000	6.3	CLEAR1L	F435W	08948, 10369, 10732, 11045, 11881
32,000	9.5	CLEAR1L	F435W	08948, 10369, 10732, 11045, 11881
42,000	12.5	CLEAR1L	F435W	08948, 10732, 11045, 11881, 12386, 12731, 13156, 13593, 13956, 14399, 14508, 14950, 15523
52,000	15.0	CLEAR1L	F435W	08948